Chemical Science

ROYAL SOCIETY OF CHEMISTRY

EDGE ARTICLE

View Article Online
View Journal | View Issue

Cite this: *Chem. Sci.*, 2024, **15**, 17685

All publication charges for this article have been paid for by the Royal Society of Chemistry

Received 25th May 2024
Accepted 15th September 2024

DOI: 10.1039/d4sc03430a

rsc.li/chemical-science

Copper catalyzed benzylic sp^3 C–H alkenylation†

Ting-An Chen,[ab] Richard J. Staples [b] and Timothy H. Warren *[b]

The prenyl group is present in numerous biologically active small molecule drugs and natural products. We introduce benzylic C–H alkenylation of substrates Ar-CH_3 with alkenylboronic esters $(CH_2)_3O_2B$–$CH{=}CMe_2$ as a pathway to form prenyl functionalized arenes Ar-$CH_2CH{=}CMe_2$. Mechanistic studies of this radical relay catalytic protocol reveal diverse reactivity pathways exhibited by the copper(II) alkenyl intermediate [Cu^{II}]-$CH{=}CMe_2$ that involve radical capture, bimolecular C–C bond formation, and hydrogen atom transfer (HAT).

Introduction

The prenyl group (–$CH_2CH{=}CMe_2$) is a prevalent functionality found in natural products and biologically active small molecules.[1–6] Prenyltransferase, an essential enzyme involved in prenylation, enhances protein stability and anchors proteins to cell membranes due to the hydrophobic nature of the prenyl group.[7–10] The addition of a prenyl group to molecules can influence their biological activities.[11–14] For instance, the prenyl group is the primary inhibitory component of the HIV inhibitor Osthol (Fig. 1a).[15] Additionally, both experimental and computational methods have been used to determine that prenylated chrysin functions as a more potent inhibitor for P-glycoprotein, a determinant of drug accumulation in leukemia cells.[16,17]

Methods for installing prenyl groups onto aromatic rings typically involve C–C coupling through allylation of an aryl halide (or pseudohalide) (Fig. 1b). For instance, Pd catalyzed Suzuki or Negishi coupling reactions produce prenylated aryl derivatives.[18–20] Alternatively, sp^2 C–H prenylation of arene C–H bonds with 1,1-dimethylallene also leads to aryl prenyl derivatives.[21–24]

This report presents an alternative strategy to prenyl-functionalized molecules through C–H alkenylation of benzylic C–H bonds *via* the alkenylboronic ester $(CH_2)_3O_2B$–$CH{=}CMe_2$ (Fig. 1d). Previous examples of direct sp^3 C–H alkenylation with alkenylboronic esters required highly acidic C–H bonds in aryl difluoromethyl derivatives Ar-CF_2H.[25] Alternatively, benzylic sp^3 C–H styrenylation occurs with styrenyl carboxylates and nitrites in the presence of ^{t}BuO^{t}Bu (Fig. 1c).[26–30]

This report utilizes the dimethylethenyl (–$CH{=}CMe_2$) group as the alkenyl source for sp^3 C–H functionalization. Our research team and other groups have employed radical relay approaches for C–H functionalization (Fig. 2a).[31–35] Based on sp^3 C–H alkynylation,[36] arylation,[37–39] and methylation[40] that proceed *via* [Cu^{II}]-C≡CAr, [Cu^{II}]-Ar, and [Cu^{II}]-Me intermediates, respectively (Fig. 2b), we anticipated that [Cu^{II}]-$CH{=}CMe_2$ intermediates (Fig. 2c) could lead to benzylic sp^3 C–H alkenylation. This would convert an Ar–CH_2–H group to Ar–CH_2–$CH{=}CMe_2$, enabling net prenylation (Fig. 1d).

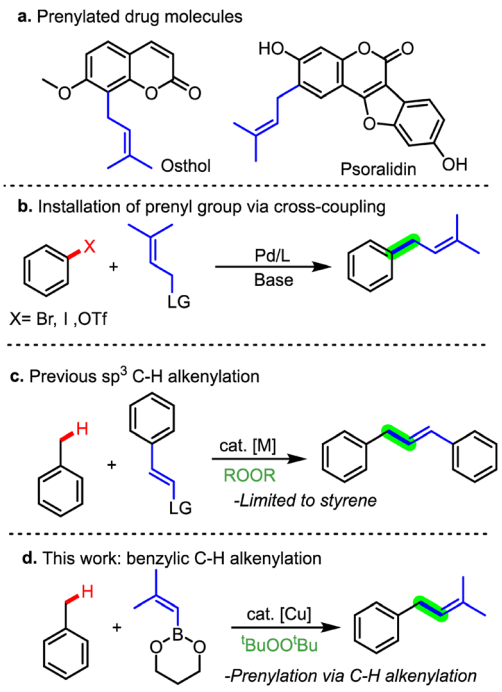

Fig. 1 (a) Prenylated natural products and drug molecules. (b) Prenylation *via* cross-coupling. (c) sp^3 C–H styrenylation. (d) Net prenylation *via* benzylic C–H alkenylation.

[a]*Department of Chemistry, Georgetown University, Washington, D.C. 20057, USA*
[b]*Department of Chemistry, Michigan State University, East Lansing, Michigan 48824, USA. E-mail: warre155@msu.edu*

† Electronic supplementary information (ESI) available. Detailed experimental procedures are provided. CCDC 2268882 2329536. For ESI and crystallographic data in CIF or other electronic format see DOI: https://doi.org/10.1039/d4sc03430a

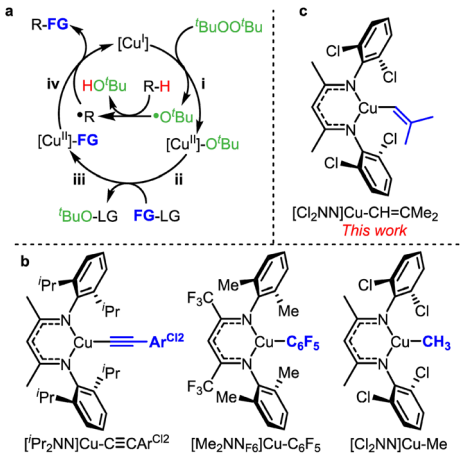

Fig. 2 (a) Radical relay mechanism for C–H functionalization. (b) β-Diketiminato copper(II) intermediates in C–H alkynylation, arylation and methylation. (c) Proposed copper(II) alkenyl intermediate for C–H alkenylation.

Results and discussion

Reaction discovery and optimization

We sought to enable benzylic C–H alkenylation, employing toluene as a representative benzylic substrate using Cu(I) β-diketiminato complexes as catalysts along with di-*tert*-butyl peroxide (^{t}BuOO^{t}Bu) as the oxidant. We chose alkenylboronic esters as the alkenyl source but recognized that the nature of the boronic ester backbone could play an important role (Scheme 1). For example, 4,4,6-trimethyl-2-phenyl-1,3,2-dioxaborinane exhibited a higher yield in sp^3 C–H arylation compared to phenylboronic acid pinacol ester.[39] Therefore, we investigated 2-alkenyl-1,3,2-dioxaborinane (**2a**) and 4,4,6-trimethyl-2-alkenyl-1,3,2-dioxaborinane (**2b**) as possible alkenyl group transfer reagents for C–H alkenylation of toluene (Scheme 1). Use of the less sterically hindered boronic ester **2a** produced a higher C–H alkenylation yield of product **3a** than with the more sterically hindered boronic ester **2b** (63% *vs.* 15%, respectively). Importantly, the more hindered boronic ester **2b** led to toluene C–H etherification to give PhCH$_2$-O^{t}Bu that signals capture of the benzyl radical PhCH$_2^\bullet$ by the [Cu^{II}]-O^{t}Bu intermediate (Scheme S1†).[41] We hypothesize that a higher rate of transmetalation between the [Cu^{II}]-O^{t}Bu intermediate and the less sterically hindered alkenylboronic ester **2a** to form a [Cu^{II}]–C=CMe$_2$ intermediate inhibits the formation of PhCH$_2$O^{t}Bu (Scheme S1†).

Employing boronic ester **2a**, we explored various parameters including the solvent, catalyst loading (Table S1†), oxidant (Table S2†), temperature (Table S4†). Using optimized conditions (10 mol% [Cu^I], 2 equiv. ^{t}BuOO^{t}Bu, 20 equiv. R–H, 300 μL benzene, and 60 °C), we also examined different copper β-diketiminate catalysts with diverse electronic and steric properties (Table 1). Among the tested catalysts, [Cl$_2$NN]Cu (Table 1, entry 1) gave the highest product yield. Interestingly, a very electron-poor catalyst (Table 1, entry 2) gave a very low yield, yet catalysts with electron-donating groups on the β-diketiminato *N*-aryl rings also decreased the product yield.

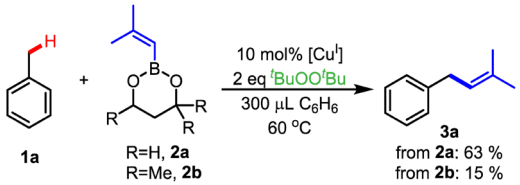

Scheme 1 Size of alkenylboronic ester impacts alkenylation yield.

Table 1 Catalyst optimization for C–H alkenylation[a]

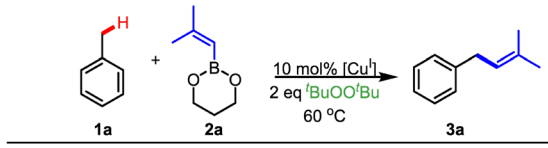

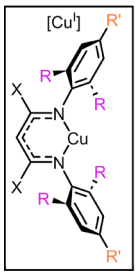

Entry	X	R	R'	Product
1	CH_3	Cl	H	63%
2	CF_3	Cl	H	6%
3	CH_3	Me	H	41%
4	CH_3	Me	Me	29%
5	CH_3	OMe	H	21%

[a] Conditions: 20 equiv. R–H, 2 equiv. ^{t}BuOO^{t}Bu, 60 °C, 1 h. Yield determined by GCMS anaiysis.

Benzylic C–H alkenylation leading to net prenylation

We systematically examined a range of benzylic R–H substrates, assessing reaction yields *via* GCMS analysis (Table 2). We initially focused on sp^3 C–H alkenylation of commercially available 1° benzylic substrates Ar-CH$_3$ that lead to prenyl derivatives ArCH$_2$–CH=CMe$_2$ (**3a–3i**) in 42–92% yield. Slightly higher yields result in more electron-rich substrates Ar-CH$_3$ (**3b**, **3d**, **3e**; 64–92%). This method tolerates aryl halides Ar-X (**3f–3h**) that typically serve as substrates in more traditional cross-coupling reactions. The method also tolerates ortho-substitution as illustrated by the use of *o*-chlorotoluene and *o*-xylene (**3i** and **3j**) for C–H alkenylation. Secondary benzylic C–H sites in ethylbenzene also undergo C–H alkenylation (**3l**), yet exhibit lower yields due to the formation of styrene in 20% yield *via* β-H-atom abstraction from the ethylbenzene radical (PhCH(•)Me) (ESI, Section 4 and Scheme S5†). Additionally, *N*,*N*-dimethyl aniline (**3o**) proved amenable to α-N C–H functionalization, albeit in lower yield (22%). We also examined indoles with heteroaryl-Me groups, but unfortunately no C–H alkenylation occurs, even with *N*-Boc protected indoles.

To highlight potential advantages of prenylation *via* benzylic C–H alkenylation, we performed C–H alkenylation on three pharmaceutically relevant compounds (**3p–3r**). Notably, our method exhibited high selectivity for benzylic C–H bonds. For example, in the case of nabumetone (**3p**) which possesses multiple sp^3 C–H bonds, exclusive benzylic C–H functionalization occurs. Entry **3r** yielded a product closely related to its *o*-OMe derivative with HIV inhibitory properties, highlighting the

Table 2 Cu catalysed C–H alkenylation[a]

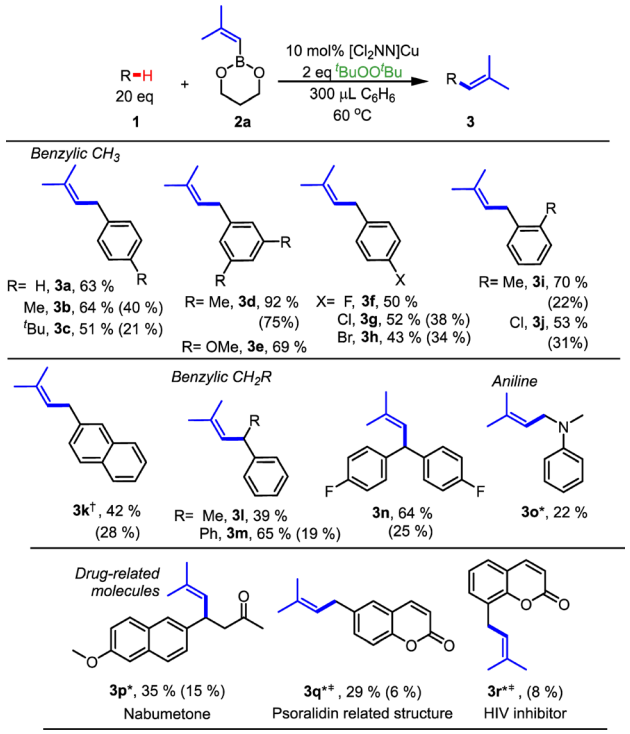

[a] Detailed reaction conditions in ESI. Yields determined by GCMS. Isolated yield in parenthesis. †80 °C. ≠ 100 °C. *10 equiv. R–H substrate used.

potential of this direct C–H alkenylation method to condense lengthy syntheses.[15] Yet we recognize the rather modest yields for the C–H functionalization step with these compounds (Table 2, entries **3p–3r**); some substrates lead to relatively strong binding with the [Cu^{I}] catalyst that impedes C–H functionalization (Scheme S2 and Fig. S4†).

Mechanistic investigations

To gain more insight into the interaction between the alkenylboronic ester and the [Cu^{I}] catalyst as well as the formation and reactivity of the proposed [Cu^{II}]-CH=CMe$_2$ intermediate, we examined facets of the reaction mechanism by integrating both experimental and computational analyses.

Alkenylboronic ester binding to copper(I) catalyst

Given the need for mild heating to encourage C–H alkenylation, we considered the possibility of equilibrium binding of the dimethylethenylboronic ester **2a** with the [Cu^{I}] catalyst (Fig. 3a). The crystal structure of the [Cu^{I}](η^2-**2a**) adduct reveals an interaction between the π electrons of the alkene and the [Cu^{I}] catalyst (Fig. 3b). Higher temperatures promote the dissociation of this adduct, leading to increased concentrations of the dissociated species. A van't Hoff plot reveals thermodynamic parameters corresponding to this equilibrium: ΔG_{exp} (298) = 6.7 ± 1.0, ΔH_{exp} = 11.1 ± 0.5 kcal mol^{-1}, and ΔS_{exp} = 14.4 ± 1.6 e.u. (Fig. 3c and S2†).

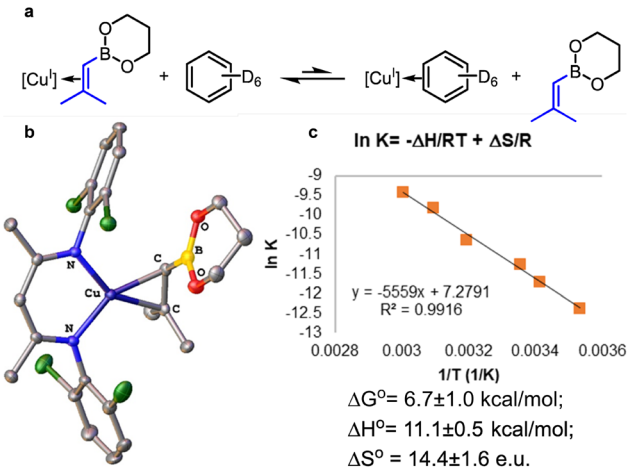

Fig. 3 (a) Reversible binding of **2a** to [Cu^{I}] catalyst in benzene, (b) X-ray structure of alkenylboronic ester adduct, and (c) van't Hoff plot.

Formation and reactivity of alkenyl intermediate [Cu^{II}]–C=CMe$_2$

Mixing [Cu^{II}]-O^{t}Bu with **2a** in fluorobenzene produces a substantial amount of 2,5-dimethylhexa-2,4-diene (alkenyl dimer) (84% yield, Fig. 4a). This could proceed *via* a [Cu^{II}]-CH=CMe$_2$ intermediate that undergoes bimolecular C–C coupling to give the observed alkenyl dimer, much as [Cu^{II}]–C≡CAr and [Cu^{II}]-Ar intermediates readily form ArC≡C-C≡CAr[37] and Ar–Ar[38] species. *In situ* UV-vis analysis was employed to monitor the reaction intermediate of [Cu^{II}]-O^{t}Bu and **2a** (Fig. S6†). Upon introducing **2a** into the [Cu^{II}]-O^{t}Bu solution at −38 °C, a rapid reaction occurred, leading to a decrease in the absorption band of [Cu^{II}]-O^{t}Bu without the detection of any newly generated [Cu^{II}] species. Based on previous bimolecular C–C bond formation *via* [Cu^{II}]–C≡CAr[37] and [Cu^{II}]-Ar[38] species, we propose that the [Cu^{II}]-CH=CMe$_2$ intermediate similarly undergoes rapid bimolecular C–C coupling to form Me$_2$C=CH–CH=CMe$_2$. Indeed, it is possible for a conjugated diene to bridge between two β-diketiminato [Cu^{I}] to form a [Cu^{I}]$_2$(μ-diene) species (Fig. S8†).

To further confirm the reaction intermediate obtained upon addition of alkenylboronic ester **2a** with [Cu^{II}]-O^{t}Bu as [Cu^{II}]-CH=CMe$_2$, reaction in the presence of Gomberg's dimer (that

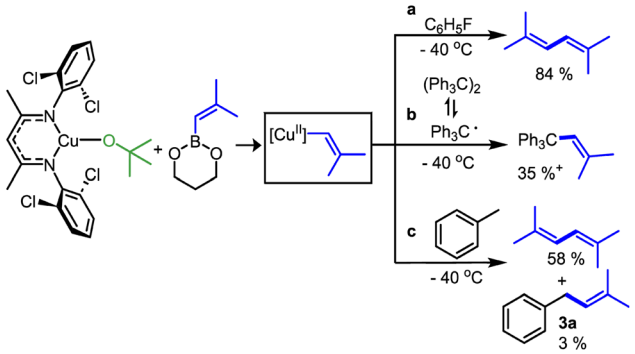

Fig. 4 Reaction of [Cl$_2$NN]Cu-O^{t}Bu and **2a** (a) in C$_6$H$_5$F, (b) in the presence of Gomberg's dimer in C$_6$H$_5$F, and (c) in toluene. +isolated yield.

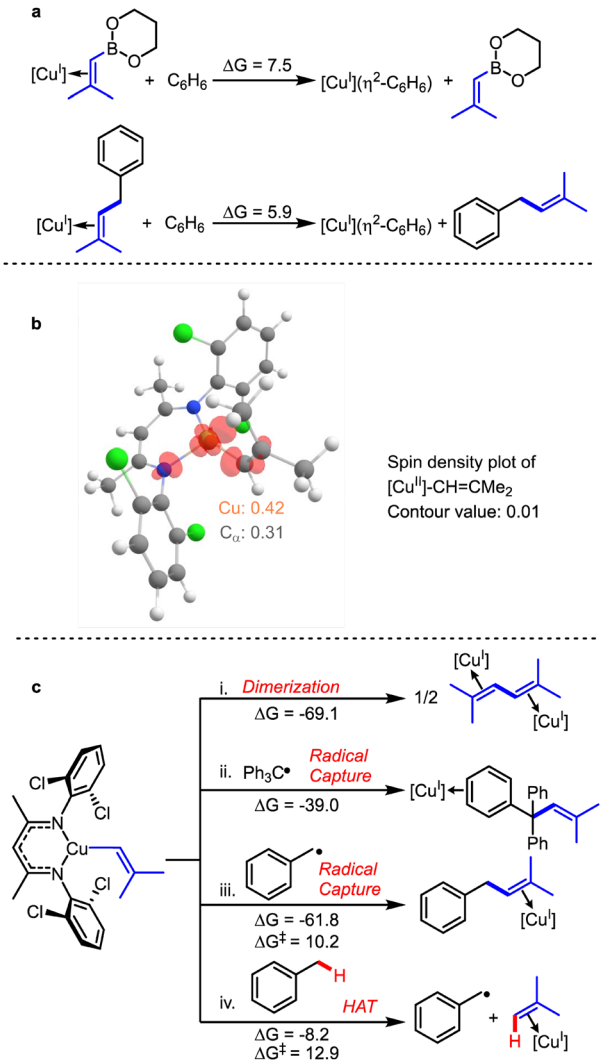

Fig. 5 DFT calculation of (a) [Cu^{I}] binds to alkenes, **2a** and **3a**. (b) spin density plot of [Cu^{II}]-CH=CMe$_2$. (c) Possible reaction pathways for [Cu^{II}]-CH=CMe$_2$. Free energies in kcal mol^{-1} at 298.15 K. For more details, see Schemes S3 and S4.

dissociates to produce the trityl radical Ph$_3$C$^{\bullet}$) provides Ph$_3$C–CH=Me$_2$ in 35% yield (Fig. 4b). Additionally, a minimal amount of **3a** also forms when the reaction occurs in toluene (Fig. 4c). Product **3a** can arise from the sequential steps of toluene radical formation through HAT, followed by subsequent radical capture (Fig. 5c).

Computational analysis and insights

We employed density functional theory (DFT) to better understand and interpret the above experimental findings. Remarkably, the experimental thermodynamic parameters derived from the van't Hoff plot for the binding of the alkenylboronic ester to [Cu^{I}], closely correspond to the predictions from density functional theory (DFT), with $\Delta G_{DFT} = 7.5$ kcal mol^{-1}, $\Delta H_{DFT} = 11.5$ kcal mol^{-1}, and $\Delta S_{DFT} = 12.1$ e.u. (Fig. 5a). The strong agreement between experimental data ($\Delta G_{exp} = 6.7 \pm 1.0$ kcal mol^{-1}) and DFT results supports the reliability of the thermodynamic data from calculations. Furthermore, the alkenylated product **3a** exhibits a lower affinity for binding to [Cu^{I}] compared to **2a** ($\Delta G_{DFT} = 5.9$ kcal mol^{-1}) (Scheme S4†).

This result is consistent with the need for mild heating (60 °C) to disrupt the interaction between alkenyl precursors or products **2a** or **3a** and the [Cu^{I}] catalyst, thereby initiating the catalytic cycle. Upon dissociation of the alkene from the [Cu^{I}] catalyst, the [Cu^{I}] complex undergoes oxidation by ^{t}BuOO^{t}Bu which requires on an accessible coordination site. Furthermore, the formation of [Cu^{II}]-CH=CMe$_2$ *via* transmetalation of [Cu^{II}]-O^{t}Bu with **2a** is exergonic ($\Delta G = -3.5$ kcal mol^{-1}) with a modest reaction barrier ($\Delta G^{\ddagger} = 13.6$ kcal mol^{-1}) (Scheme S3†).

A spin density plot of the [Cu^{II}]-CH=CMe$_2$ intermediate indicates 31% localization on C$_\alpha$ (Fig. 5b). The radical nature of the alkenyl group bound to the copper(II) center in [Cu^{II}]-CH=CMe$_2$ also accounts for its propensity to dimerize to form Me$_2$C=CH–CH=CMe$_2$, a highly favorable reaction ($\Delta G_{rxn} = -69.1$ kcal mol^{-1}). A relaxed energy scan for dimerization further reveals essentially no barrier for this process (Fig. S22†). Similarly, the radical capture by trityl radical pathway is also a highly favourable reaction ($\Delta G = -39.0$ kcal mol^{-1}) (Fig. 5c(ii)). We note that loss of the alkenyl radical $^{\bullet}$CH=CMe$_2$ from [Cu^{II}]-CH=Me$_2$ is significantly uphill in free energy ($\Delta G = 36.0$ kcal mol^{-1}; Fig. S21†); accordingly we do not anticipate the direct involvement of the $^{\bullet}$CH=CMe$_2$ radical in these copper-catalyzed reactions.

Due to the radical character on C$_\alpha$, we investigated whether [Cu^{II}]-CH=CMe$_2$ could abstract a H-atom from a benzylic C–H bond. This HAT process is favourable with a relatively low reaction barrier ($\Delta G = -8.2$ kcal mol; $\Delta G^{\ddagger} = 12.9$ kcal mol; Fig. 5v(iv)). This calculation result is consistent with the experiment, where a trace amount of alkenylation product, 3a, was observed in the absence of ^{t}BuO$^{\bullet}$ (Fig. 4c). After [Cu^{II}]-CH=CMe$_2$ abstracts an H atom from toluene, the resulting toluene radical undergoes capture by [Cu^{II}]-CH=CMe$_2$ to form **3a** (Fig. 5c(iii)). Calculations also rationalize the formation of styrene as a byproduct in the C–H alkenylation of ethylbenzene. Both radical capture and H-atom abstraction of a β-H of the 2° ethylbenzene radical PhCH($^{\bullet}$)Me are extremely favorable ($\Delta G = -55.0$ and -48.3 kcal mol^{-1}, respectively; Scheme S5†).

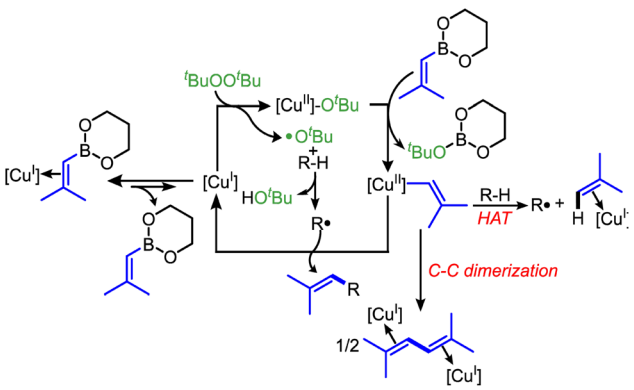

Scheme 2 Catalytic cycle for sp^3 C–H alkenylation with competing pathways *via* the [Cu^{II}]-CH=CMe$_2$ intermediate.

Conclusions

This report illustrates the use of alkenylboronic esters in catalytic benzylic C–H functionalization for sp^3–sp^2 C–C bond construction. The $Me_2C{=}CH{-}B(OR)_2$ reagent **2a** exhibits a broad C–H substrate scope across typical 1° benzylic C–H bonds. Importantly, it significantly expands the scope for benzylic C–H alkenylation as it does not require highly acidified $ArCF_2$-H bonds.[25] Importantly, this study illustrates how sp^3 C–H alkenylation can lead to formation of the prenyl group known to engender biological activity in small molecules.

A combination of experimental and computational studies support that this sp^3 C–H alkenylation protocol proceeds *via* a copper(II) alkenyl intermediate $[Cu^{II}]$-CH=CMe_2 (Scheme 2). This $[Cu^{II}]$-CH=CMe_2 intermediate promotes C–C bond formation to form R–CH=CMe_2 products in the capture of an alkyl radical R$^\bullet$ derived from H-atom abstraction from R–H *via* the ^{t}BuO$^\bullet$ radical generated upon reaction of ^{t}BuOO^{t}Bu with $[Cu^I]$. Facile bimolecular C–C coupling between $[Cu^{II}]$-CH=CMe_2 species results in a competing pathway to form the diene $Me_2C{=}CH{-}CH{=}CMe_2$. Yet, the copper(II) alkenyl intermediate can also directly transform substrates R–H into R–CH=CMe_2, albeit in low yield, due to the ability of the $[Cu^{II}]$-CH=CMe_2 intermediate to abstract a H-atom from substrates R–H to form R$^\bullet$. This unusual chemical pathway available uncovered for copper(II) alkenyls offers additional opportunities to construct catalytic C–H alkenylation protocols *via* selective H-atom abstraction of substrates R–H *via* metal-centred intermediates en route to functionalized species R–CH=CRR′.

Data availability

All synthetic procedures, characterization data, spectroscopic data, computational data, supplementary figures and tables, and detailed crystallographic information can be found in the ESI. Crystallographic data are available *via* the Cambridge Crystallographic Data Centre (CCDC): 2268882 and 2329536.

Author contributions

T.-A. C. and T. H. W. conceived project. T.-A. C. carried out experimental and computational works. T.-A. C. and R. J. S. collected, solved, and refined crystallographic data. T. H. W. supervised the experimental and computational work. T.-A. C. and T. H. W. wrote the manuscript. All authors have given approval to the final version of the manuscript.

Conflicts of interest

There are no conflicts to declare.

Acknowledgements

We are grateful to NSF (CHE-1955942 and CHE-2303206) for supporting this work. The Rigaku Synergy S Diffractometer was purchased with support of the NSF MRI program (CHE-1919565). Dr Daniel Holmes for help in variable temperature NMR experiments, and Dr Anthony Schilmiller for insightful discussions regarding HRMS analyses as well as Nathan Slater and Dr Xingling Pan for synthetic assistance.

Notes and references

1 M. E. G. Mosquera, G. Jiménez, V. Tabernero, J. Vinueza-Vaca, C. García-Estrada, K. Kosalková, A. Sola-Landa, B. Monje, C. Acosta, R. Alonso and M. Á. Valera, *Sustainable Chem.*, 2021, **2**, 467–492.
2 J. D. Ochocki and M. D. Distefano, *Med. Chem. Commun.*, 2013, **4**, 476–492.
3 K. Šmejkal, *Phytochem. Rev.*, 2014, **13**, 245–275.
4 M. E. Tanner, *Nat. Prod. Rep.*, 2014, **32**, 88–101.
5 X. Yang, Y. Jiang, J. Yang, J. He, J. Sun, F. Chen, M. Zhang and B. Yang, *Trends Food Sci. Technol.*, 2015, **44**, 93–104.
6 R. Ciochina and R. B. Grossman, *Chem. Rev.*, 2006, **106**, 3963–3986.
7 P.-H. Liang, T.-P. Ko and A. H.-J. Wang, *Eur. J. Biochem.*, 2002, **269**, 3339–3354.
8 D. P. Labbé, S. Hardy and M. L. Tremblay, *Prog. Mol. Biol. Transl. Sci.*, 2012, **106**, 253–306.
9 C. C. Palsuledesai and M. D. Distefano, *ACS Chem. Biol.*, 2015, **10**, 51–62.
10 E. S. Marakasova, N. K. Akhmatova, M. Amaya, B. Eisenhaber, F. Eisenhaber, M. L. van Hoek and A. V. Baranova, *Mol. Biol.*, 2013, **47**, 622–633.
11 B. Botta, A. Vitali, P. Menendez, D. Misiti and G. D. Monache, *Curr. Med. Chem.*, 2005, **12**, 713–739.
12 M. M. M. Pinto, M. E. Sousa and M. S. J. Nascimento, *Curr. Med. Chem.*, 2005, **12**, 2517–2538.
13 K. Yazaki, K. Sasaki and Y. Tsurumaru, *Phytochemicals*, 2009, **70**, 1739–1745.
14 X. Chen, E. Mukwaya, M.-S. Wong and Y. Zhang, *Pharm. Biol.*, 2014, **52**, 655–660.
15 S. Tamura, T. Fujitani, M. Kaneko and N. Murakami, *Bioorg. Med. Chem. Lett.*, 2010, **20**, 3717–3720.
16 G. Comte, J.-B. Daskiewicz, C. Bayet, G. Conseil, A. Viornery-Vanier, C. Dumontet, A. Di Pietro and D. Barron, *J. Med. Chem.*, 2001, **44**, 763–768.
17 R. Badhan and J. Penny, *Eur. J. Med. Chem.*, 2006, **41**, 285–295.
18 Y. Yang and S. L. Buchwald, *J. Am. Chem. Soc.*, 2013, **135**, 10642–10645.
19 Y. Yang, T. J. L. Mustard, P. H.-Y. Cheong and S. L. Buchwald, *Angew. Chem., Int. Ed.*, 2013, **52**, 14098–14102.
20 J. L. Farmer, H. N. Hunter and M. G. Organ, *J. Am. Chem. Soc.*, 2012, **134**, 17470–17473.
21 M. A. Tarselli, A. Liu and M. R. Gagné, *Tetrahedron*, 2009, **65**, 1785–1789.
22 Y. J. Zhang, E. Skucas and M. J. Krische, *Org. Lett.*, 2009, **11**, 4248–4250.
23 S.-Y. Chen, Q. Li and H. Wang, *J. Org. Chem.*, 2017, **82**, 11173–11181.
24 R. Zeng, C. Fu and S. Ma, *J. Am. Chem. Soc.*, 2012, **134**, 9597–9600.

25 K. Chakrabarti, M. M. W. Wolfe, S. Guo, J. W. Tucker, J. Lee and N. K. Szymczak, *Chem. Sci.*, 2024, **15**, 1752–1757.
26 S. Guo, Y. Yuan and J. Xiang, *New J. Chem.*, 2015, **39**, 3093–3097.
27 Z. Fang, C. Wei, J. Lin, Z. Liu, W. Wang, C. Xu, X. Wang and Y. Wang, *Org. Biomol. Chem.*, 2017, **15**, 9974–9978.
28 Z. Cui, X. Shang, X.-F. Shao and Z.-Q. Liu, *Chem. Sci.*, 2012, **3**, 2853–2858.
29 H. Yang, P. Sun, Y. Zhu, H. Yan, L. Lu, X. Qu, T. Li and J. Mao, *Chem. Commun.*, 2012, **48**, 7847–7849.
30 H. Yang, H. Yan, P. Sun, Y. Zhu, L. Lu, D. Liu, G. Rong and J. Mao, *Green Chem.*, 2013, **15**, 976–981.
31 D. L. Golden, S.-E. Suh and S. S. Stahl, *Nat. Rev. Chem*, 2022, **6**, 405–427.
32 Z. Zhang, P. Chen and G. Liu, *Chem. Soc. Rev.*, 2022, **51**, 1640–1658.
33 E. S. Jang, C. L. McMullin, M. Käß, K. Meyer, T. R. Cundari and T. H. Warren, *J. Am. Chem. Soc.*, 2014, **136**, 10930–10940.
34 M. S. Kharasch and G. Sosnovsky, *J. Am. Chem. Soc.*, 1958, **80**, 756.
35 M. S. Kharasch, G. Sosnovsky and N. C. Yang, *J. Am. Chem. Soc.*, 1959, **81**, 5819–5824.
36 A. Bakhoda, O. E. Okoromoba, C. Greene, M. R. Boroujeni, J. A. Bertke and T. H. Warren, *J. Am. Chem. Soc.*, 2020, **142**, 18483–18490.
37 S. Kundu, C. Greene, K. D. Williams, T. K. Salvador, J. A. Bertke, T. R. Cundari and T. H. Warren, *J. Am. Chem. Soc.*, 2017, **139**, 9112–9115.
38 W. Xie, J. Heo, D. Kim and S. Chang, *J. Am. Chem. Soc.*, 2020, **142**, 7487–7496.
39 A. Vasilopoulos, S. L. Zultanski and S. S. Stahl, *J. Am. Chem. Soc.*, 2017, **139**, 7705–7708.
40 B. C. Figula, T.-A. Chen, J. A. Bertke and T. H. Warren, *ACS Catal.*, 2022, **12**, 11854–11859.
41 R. T. I. Gephart, C. L. McMullin, N. G. Sapiezynski, E. S. Jang, M. J. B. Aguila, T. R. Cundari and T. H. Warren, *J. Am. Chem. Soc.*, 2012, **134**, 17350–17353.